ORIGINAL ARTICLE

Evelyn Mayaan · Kevin Range · Darrin M. York

Structure and binding of Mg(II) ions and di-metal bridge complexes with biological phosphates and phosphoranes

Abstract Divalent Mg^{2+} ions often serve as cofactors in enzyme or ribozyme-catalyzed phosphoryl transfer reactions. In this work, the interaction of Mg^{2+} ions and di-metal bridge complexes with phosphates, phosphoranes, and other biological ligands relevant to RNA catalysis are characterized with density functional methods. The effect of bulk solvent is treated with two continuum solvation methods (PCM and COSMO) for comparison. The relative binding affinity for different biological ligands to Mg^{2+} are quantified in different protonation states. The structure and stability of the single-metal and di-metal complexes are characterized, and the changes in phosphate and phosphorane geometry induced by metal ion binding are discussed. Di-metal bridge complexes are a ubiquitous motif and the key factors governing their electrostatic stabilization are outlined. The results presented here provide quantitative characterization of metal ion binding to ligands of importance to RNA catalysis, and lay the groundwork for design of new generation quantum models that can be applied to the full biological enzymatic systems.

Abbreviations DMPH: dimethyl hydrogen phosphate · EP^-: ethylene phosphate · EPA^{2-}: methyl(ethylene)phosphorane · $EPAH^-$: methyl(ethylene)(hydrogen)phosphorane · EPH: ethylene hydrogen phosphate

E. Mayaan · K. Range · D. M. York (✉)
Department of Chemistry, University of Minnesota,
207 Pleasant Street SE, Minneapolis,
MN 55455-0431, USA
E-mail: york@chem.umn.edu
Tel.: +1-612-6248042
Fax: +1-612-6267541

Introduction

Metal ion binding to RNA plays a fundamental role in biological phosphate hydrolysis reactions [1, 2]. Understanding the chemical properties and reactivity of phosphates is of critical importance to determining how these biomolecules are formed and cleaved. The theoretical study of metal ion interactions with biological ligands has been of great interest in recent years [3, 4, 5, 6]. Although phosphate diesters have been the subject of numerous theoretical and experimental studies [7, 8, 9, 10, 11, 12], phosphate hydrolysis occurring through metal ion assisted catalysis has received relatively less attention [13, 14, 15, 16]. However, the abundance of experimental studies now available for biologically occurring ribozymes, such as hammerhead and RNase P, continue to reveal the importance of metal ions to RNA phosphate hydrolysis [17, 18, 19, 20, 21, 22]. In the hammerhead ribozyme, for instance, phosphate hydrolysis occurs 10,000 times faster in the presence of 10 mM Mg^{2+} [19]. Understanding the mechanistic details behind this rate enhancement is of critical importance to further applications, such as drug development for gene related diseases [23].

Metal ions are assumed to aid in catalysis through structural stabilization of active conformations and reactive intermediates/transition states. In some cases they seem to play a chemical role as well, involving reaction initiation through proton transfer [13, 19, 24, 25, 26, 27]. It is of interest to determine how ribozyme conformational changes are induced and stabilized upon metal ion binding [20, 28, 29]. However, computational study of metal-assisted phosphate hydrolysis reactions is very challenging due to the large size, high charge, and conformational flexibility of RNA. As such, accurate theoretical study of these systems is largely infeasible with many current conventional techniques and models. A promising approach is to use hybrid quantum mechanical/molecular mechanical (QM/MM) methods [30, 31, 32, 33]. This technique

uses an accurate but time-consuming quantum model to study the detailed chemical transformations of the active site. Meanwhile, the remainder of the system is treated with a less accurate but more computationally feasible classical empirical force field. The development of a quantum model such as this for metal-assisted phosphate hydrolysis reactions is an important step towards the accurate theoretical study of ribozyme systems. The objective of the present paper is to extend the scope of previous theoretical studies of biological phosphates and phosphoranes [10] to include a systematic study of the binding of Mg^{2+} ions to these and other biological ligands, as well as to investigate the structure and stability of di-metal bridge complexes similar to those observed in ribozymes and polymerase enzymes. These results offer valuable insight into the structure and energetics of these metal ion interactions and provide useful information for the construction of accurate new quantum methods for use with QM/MM modeling [34, 35] of biological reactions that involve Mg^{2+} ions.

Methods

Gas-phase calculations

All calculations were performed with the GAUSSIAN 03 [36] package using Kohn-Sham density functional theory (DFT) with the hybrid Becke three-parameter exchange functional [37] and the Lee, Yang, Parr correlation functional (B3LYP) [38]. Geometry optimizations were performed with the 6-31++G(d,p) basis set [39] and stability conditions of the restricted closed shell Kohn-Sham determinant for each final structure were verified [40, 41]. Frequency calculations were performed to establish the nature of all stationary points and allow evaluation of the thermodynamic quantities of interest. Electronic energies were further refined using the 6-311++G(3df,2p) basis set, which is similar to that used in the G2 [42] method.

Solvation calculations

Solvation effects were treated by single-point calculations based on the gas-phase optimized structures using the polarizable continuum model (PCM) [43, 44, 45, 46] and a variation of the conductor-like screening model (COSMO) [47, 48, 49] as implemented in GAUSSIAN 03.

The solvation free energy, ΔG_{sol}, is defined as:

$$\Delta G_{sol} = G_{aq} - G_{gas} \qquad (1)$$

where G_{gas} and G_{sol} are the molecular free energies in the gas phase and in solution, respectively. In the present work the approximation is made that the gas-phase geometry, entropy, and thermal corrections to the enthalpy do not change upon solvation. The

practical reason for introducing this approximation resides in the difficulty and considerable computational cost associated with obtaining stationary points and Hessians with the boundary element solvation methods. Within these approximations, the solvation energy is given by:

$$\Delta G_{sol} = (E[\Psi_{sol}] + E_{sol}[\rho_{sol}]) - E[\Psi_{gas}] \qquad (2)$$

where $E[\Psi_{gas}]$ and $E[\Psi_{sol}]$ are the the Kohn-Sham energy functionals that take as arguments the Kohn-Sham single-determinant wavefunction optimized in the gas phase (Ψ_{gas}) and in solution (Ψ_{sol}), and $E_{sol}[\rho_{sol}]$ is the solvation energy that takes as argument the polarized electron density in solution $\rho_{sol}(\mathbf{r})$ (which can be derived from Ψ_{sol}).

In the PCM and COSMO models, the solvation energy functional $E_{sol}[\rho_{sol}]$ can be written as:

$$E_{sol}[\rho] = \frac{1}{2}\left(\int \rho(\mathbf{r})v_{RF}(\mathbf{r})\,d^3r - \sum_\alpha Z_\alpha v_{RF}(\mathbf{R}_\alpha)\right) + G_{disp-repul} + G_{cav} \qquad (3)$$

where $v_{RF}(\mathbf{r})$ is the solvent reaction-field potential, Z_α is the nuclear charge of atom α located at position $\mathbf{R}_\alpha$. The factor of 1/2 in Eq. 3 results from the linear-response nature of the dielectric models, and the $G_{dis-repul}$ and G_{cav} represent the dispersion-repulsion and cavitation contributions, respectively [44].

The cavitation term is computed using an expression obtained from scaled particle theory [50] with a cavity constructed from the UAKS radii [51]. The dispersion-repulsion term is calculated according to the prescription described by Floris et al. [52] with a solvent accessible surface that is constructed from the UAKS radii plus a solvent probe radius of 1.385 Å.

The difference between the PCM and COSMO methods used here resides in the way in which the solvent reaction field potential $v_{RF}(\mathbf{r})$ is generated (see [44] and [47] for details). In the case of the PCM model, a cavity of unit dielectric is surrounded by a linear isotropic polarizable continuum of dielectric constant ϵ, the reaction field potential for which is solved numerically using a boundary element method [43, 51, 53, 54]. In the conductor-like screening model [55], a similar dielectric problem that involves a surrounding conductor ($\epsilon = \infty$) is solved, in the present case using a variation of the PCM method [47], and the resulting reaction-field potential is corrected approximately for the finite external dielectric ϵ [55, 56]. All PCM and COSMO calculations were carried out using the B3LYP/6-311++G(3df,2p) level of theory (the same level as the gas-phase single points) using the gas-phase optimized geometries.

Thermodynamic quantities

For the energetic analysis, the results are broken down into their thermodynamic contributions (see Introduc-

tion). The breakdown of the key thermodynamics relations and energy components in the gas phase are summarized below:

$$G = H - TS \tag{4}$$

$$H = U + RT \tag{5}$$

$$U = E_0 + E_{vib} + E_{rot} + E_{trans} \tag{6}$$

$$E_0 = (E_{elec} + E_{NN}) + E_{ZPV} = E + E_{ZPV} \tag{7}$$

where G, U, H, S, and T are the Gibbs free energy, internal energy, enthalpy, entropy, and absolute temperature, respectively, R is the universal gas constant, and E_{elec}, E_{NN}, E_{ZPV}, E_{vib}, E_{rot}, and E_{trans} are the electronic energy, nuclear–nuclear repulsion energy, zero-point vibrational energy, thermal vibrational energy correction, rotational and translational energy components, respectively. The expression for the enthalpy (Eq. 5) assumes the ideal gas law for a mole of particles. The internal energy and entropy were derived from standard statistical mechanical expression for separable vibrational, rotational, and translational contributions within the harmonic oscillator, rigid rotor, ideal gas/particle-in-a-box models in the canonical ensemble [57]. The standard state is for a mole of particles at $T = 298$ K and 1 atm pressure ($V = RT/P$). All quantities above except E_0, E_{elec}, and E_{ZPV} have explicit temperature dependence.

Results and discussion

Structure

Aqueous Mg^{2+} cations are generally found with six ligands bound in an octahedral manner [58, 59]. Of the four most abundant biological cations (Na^+, K^+, Ca^{2+}, Mg^{2+}), Mg^{2+} is the smallest in size and chemically hardest. While the coordination of Mg^{2+} with H_2O ligands is relatively well studied [58, 59, 60, 61], Mg^{2+} complexes with phosphates and phosphorane ligands relevant for RNA catalysis are less well characterized. In this paper, quantum results for a large dataset of Mg^{2+} complexes with biologically relevant ligands are presented, including H_2O, dimethyl phosphate (DMP$^-$), ethylene phosphate (EP$^-$), methyl(ethylene)phosphorane (EPA^{2-}), HO$^-$, CH_3O^-, and CH_3COO^-. These metal binding interactions are often crucial to phosphate hydrolysis reactions in biological systems [62, 63, 64, 65]. The dataset is analyzed in terms of molecular structures and thermodynamic quantities in gas and aqueous phase.

Mg(II) coordination with H_2O and OH$^-$

Average gas-phase optimized Mg^{2+}–O and O–H distances for a Mg^{2+} ion coordinated with various numbers of water molecules were calculated (Table S1 in Supplementary material). The average Mg^{2+}–O distance increases linearly with increasing water coordination from a minimal value of 1.938 Å for coordination with one water to 2.111 Å when fully coordinated with six water molecules (an increase of 0.173 Å). The gas-phase optimized coordination distances are slightly larger than those of other theoretical studies [58, 59, 60, 61], in part due to the inclusion of diffuse functions in the basis set used for the geometry optimization in the present work. The average gas-phase optimized coordination distance for hexacoordinated Mg^{2+} is slightly larger than the value obtained from X-ray diffraction experiments that estimate a value of 2.09 Å [66]. Re-optimization of the fully coordinated Mg^{2+} complexes using implicit solvation shows a systematic contraction of water coordination distance with the charge state of the system compared with the gas-phase optimization, leading to an average value of 2.081 Å for $[Mg(H_2O)_6]^{2+}$ with the PCM and COSMO solvation models, in closer agreement with experiment. Figure 1 shows the binding energy results for successive water additions to Mg^{2+}. These results compare well with other computational studies performed at a similar level of theory and are slightly higher in energy than results seen for studies using a MP2 or MP3 method [58, 59, 61, 67].

Substitution of H_2O with OH$^-$ in the first coordination sphere of Mg^{2+} leads to an overall increase in the Mg^{2+}–OH$_2$ coordination distance (0.020 Å and 0.093 Å increase for single and double H_2O/OH$^-$ substitutions, respectively), as well as an increase in the average Mg^{2+}–OH coordination distance. This is due in part to a Born ion-like contraction effect: the solvation energy of a charged system will increase in magnitude as the
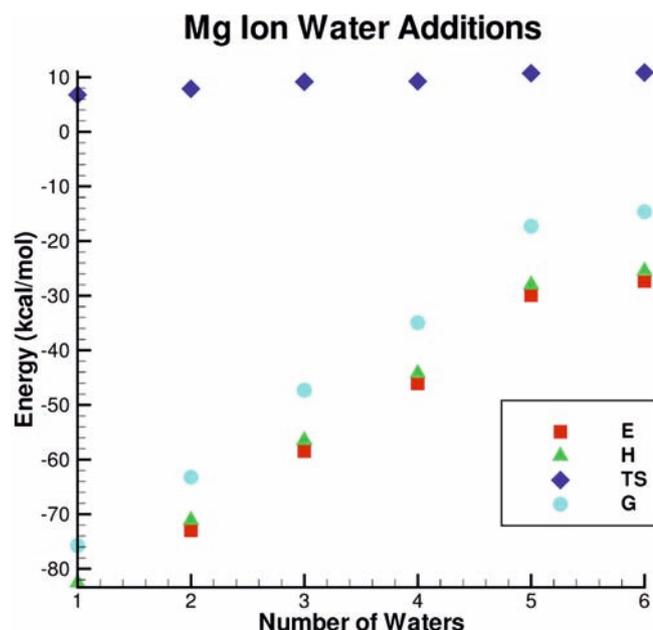
Fig. 1 Thermodynamic quantities for successive water additions for the reaction $[Mg(H_2O)_{n-1}]^{2+} + H_2O \rightarrow [Mg(H_2O)_n]^{2+}$ (see text)

square of the total charge and as the inverse of the effective radius (other factors being equal). Consequently, solvation of a charged system will tend to favor a reduced effective radius, and hence contraction of coordination distance and O–H bond length. This contraction is most pronounced for $[Mg(H_2O)_6]^{2+}$, which has the largest charge (data not shown). Coordination of OH^- is slightly tighter than that of H_2O by around 0.175–0.200 Å, especially in the case of a single coordinating hydroxide ion.

Biological ligand coordination to hydrated Mg(II)

Significant variations are seen in the coordination distances of biological ligands bound with Mg^{2+} (Table S1). Water ligands have the largest Mg^{2+} coordination distance (2.111 Å). All other monodentate ligand substitutions studied decrease in coordination distance between −0.028 Å for $[Mg(H_2O)_5(CH_3CO_2H)]^{2+}$ and −0.151 Å for $[Mg(H_2O)_5(OH)]^+$. The trend for monodentate Mg^{2+}–ligand coordination distances is:

$OH^- \approx {}^-OCH_3 <$ EPAH$^- <$ DMP$^- \approx$ EP$^- <$ HPO$_4^{2-} \approx$ CH$_3$COO$^- \approx$ H$_2$PO$_4^- <$ EPA$^{2-} \approx$ EPH $\approx$ DMPH $<$ H$_3$PO$_4 <$ CH$_3$COOH $<$ H$_2$O
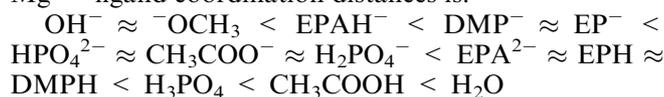
In general, anionic ligands have tighter coordination than neutral ligands, with smaller ligands such as OH^- coordinating the most tightly. Bidentate ligands have much larger coordination distances than monodentate ligands, increasing from 0.062 Å to 0.107 Å, which is even more elongated than H_2O.

Ligand-induced effects on Mg(II) structure

Upon binding to biological ligands, changes in the geometry of hydrated Mg^{2+} are observed. In most cases, H_2O ligand substitution of hexa-hydrated Mg^{2+} ion with another biological ligand causes the remaining H_2O ligands to bind less tightly (Table 1). The elongation of water coordination distances caused by biological ligand binding is correlated with the charge of the ligand: the more negatively charged the ligand, the greater the elongation. This effect is most pronounced for di-anionic ligands, with an increase in H_2O coordination distance of up to 0.038 Å as seen for EPA^{2-}. This is due in part to steric effects from the larger, more negatively charged ligand binding more tightly than the H_2O ligand it replaced, thus causing a slight displacement of the other bound H_2O ligands.

Mg(II) binding-induced effects on phosphate structure

Binding of hydrated Mg^{2+} to phosphate ligands also induces changes in the ligand geometry. Table S4 in the Supplementary material contains observed P–O bond lengths for the phosphate ligands studied. (A bridging P–O bond is one which contains an oxygen atom bonded between the a phosphorus and carbon atom. Non-

Table 1 Geometries of Mg(H$_2$O)$_5$ complexes with biological ligands

Molecule	$Mg^{2+} \cdots O_{H_2O}$ (Å)	$Mg^{2+} \cdots L$ (Å)	$Mg^{2+} \perp$
$[Mg(H_2O)_6]^{2+}$	2.111(0.000)	2.111	-
$[Mg(H_2O)_5(CH_3CO_2H)]^{2+}$	2.110(0.009)	2.083	0.00
$[Mg(H_2O)_5(H_3PO_4)]$	2.118(0.011)	2.039	32.41
$[Mg(H_2O)_5(DMPH_{g-g})]^{2+}$	2.122(0.004)	2.033	54.80
$[Mg(H_2O)_5(EPH)]^{2+}$	2.117(0.011)	2.029	2.88
$[Mg(H_2O)_5(OH)]^{1+}$	2.131(0..018)	1.956	-
$[Mg(H_2O)_5(OCH_3)]^{1+}$	2.133(0.021)	1.960	-
$[Mg(H_2O)_5(EPAH)]^{1+}$	2.124(0.023)	1.982	28.26
$[Mg(H_2O)_5(DMP_{g-g})]^{1+}$	2.124(0.016)	2.005	49.01
$[Mg(H_2O)_5(EP)]^{1+}$	2.125(0.021)	2.007	45.52
$[Mg(H_2O)_5(CH_3CO_2)]^{1+}$	2.115(0.041)	2.015	0.62
$[Mg(H_2O)_5(H_2PO_4)]^{1+}$	2.122(0.009)	2.016	7.45
$[Mg(H_2O)_5(HPO_4)]$	2.136(0.031)	2.013	15.87
$[Mg(H_2O)_5(EPA)]$	2.149(0.037)	2.029	21.50
$[Mg(H_2O)_4(b–DMP_{g-g})]^{1+}$	2.118(0.038)	2.112(0.003)	16.92
$[Mg(H_2O)_4(b–EP)]^{1+}$	2.120(0.032)	2.089(0.009)	0.07
$[Mg(H_2O)_4(b–EPA)]$	2.125(0.026)	2.091(0.068)	0.38

Shown above are the average Mg^{2+}-water and biological ligand coordination distances. For DMP compounds, the subscript *g-g* indicates the gauche-gauche conformation. Deviations are shown in parentheses. "$Mg^{2+} \perp$" refers to the Mg^{2+} angle out of plane with the surface defined by the O-P-O or O-C-O angle formed with the non-bridging oxygen and coordinating oxygen atoms

bridging refers to a P–O bond where the oxygen is either bonded to no other atoms, or else is bonded to a single hydrogen atom.) Whether protonated or unprotonated, large decreases in the bond lengths of bridging P–O bonds are observed when monodentate metal binding occurs. The effect is most pronounced for anionic phosphates, as in the case of $[Mg(H_2O)_4(b-DMP)]^+$ which decreases −0.072 Å from the 1.677 Å seen for the unbound phosphate. The effect is larger for cyclic EP$^-$ complexes then for acyclic DMP$^-$ with the largest bond contractions occurring for bidentate ligand binding. For instance, in the case of bidentate EP$^-$ coordination to Mg^{2+}, the bridging P–O bond length is shortened by −0.090 Å. There is no appreciable difference in the amount of contraction seen for *gauche-gauche* (g-g) versus *gauche-trans* (g-t) conformations of acyclic DMP$^-$. The overall length of bridging P–O bonds is slightly larger in g-g conformations than in g-t conformations. Unlike bridging phosphate P–O bonds, non-bridging bonds undergo very little change upon binding to Mg^{2+}. However, the previously non-bridging P–O bond, which coordinates with the hydrated Mg^{2+} upon binding, shows a distinct change in character. Natural bond order (NBO) analysis [68] reveals that metal binding to this O–P bond causes its bond order to be reduced by up to 0.25 units in the gas phase and 0.19 units in the aqueous phase, thus significantly lengthening the bond. This effect is slightly more pronounced for anionic phosphate ligands such as $[Mg(H_2O)_5(DMP)]^+$, which increases 0.036 Å from 1.504 Å to 1.540 Å.

Strong hydrogen bonding interactions between phosphate ligands and hydrated Mg^{2+} occurred only for

$[Mg(H_2O)_5(DMP)]^{2+}$ and $[Mg(H_2O)_5(EP)]^+$ (Fig. 2). Weaker interactions were also seen for all other monodentate Mg^{2+} phosphate complexes. In each case, hydrogen bonding occurred at one of the non-bridging oxygen positions. Weak hydrogen bonding is usually found at one of the bridging oxygen positions as well, except when Mg^{2+} is deprotonated as in $[Mg(H_2O)_4(OH)(DMP)]^+$. Bidentate phosphate ligands did not form hydrogen bonds with Mg^{2+} water ligands, possibly because the phosphate ligand is sufficiently stabilized by the double ligand binding interaction.

Mg(II) binding-induced effects on phosphorane structure

In the gas phase, di-anionic EPA^{2-} is unstable due to its high negative charge [10, 69]. However, theoretical calculations of structure and thermodynamic data have been carried out for mono-anionic and neutral phosphoranes in other work [10, 70, 71]. Binding to hydrated Mg^{2+} stabilizes this and other phosphorane ligands through direct coordination and hydrogen bonding between Mg^{2+} water ligands and phosphorane oxygens.

The length of endocyclic axial O–P bonds is sensitive to the hydrogen bonding environment (Fig. 3). In cases where a hydrogen bond is present, the O–P axial bond is stabilized and elongated. An example of this is seen for the complex of $[Mg(H_2O)_5(EPAH)]^+$, which was optimized in two different conformations, one that involved hydrogen bonding to the endocyclic axial oxygen and one that involved hydrogen bonding to the exocyclic axial oxygen. In the former case, the endocyclic O–P bond is elongated to 1.938 Å (Table 2), while in the latter case it is contracted 0.195 Å to 1.743 Å. The same effect is seen for the exocyclic axial bond as well with the O–P bond increasing from 1.650 Å to 1.740 Å when a hydrogen bond at this location is present.

For protonated phosphoranes, large contractions in the bridging equatorial P–O bonds occur upon Mg^{2+} binding. In the case of $[Mg(H_2O)_5(EPAH)]^+$, this contraction is as much as −0.066 Å. While gas-phase optimization of EPA^{2-} was not possible for comparison, PCM solution-phase optimization predicted an equatorial bridging O–P bond length of 1.714 Å for unbound

Fig. 2 $[Mg(HOH)_5(DMP)]^+$ and $[Mg(HOH)_4(b\text{-}DMP)]^+$ structures
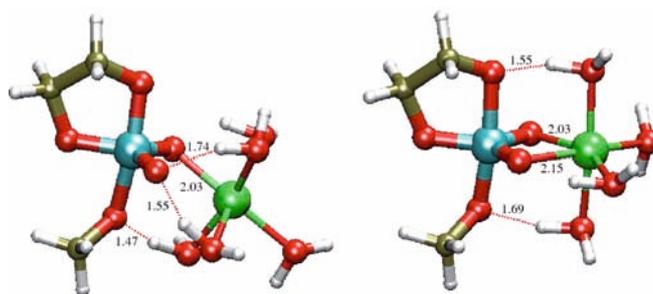
Fig. 3 $[Mg(HOH)_5(EPA)]$ and $[Mg(HOH)_5(b\text{-}EPA)]$ structures

Table 2 Geometries of phosphorane complexes with hydrated Mg2+ binding (Å)

| Molecule | equatorial | | | | axial | | | |
| | bridging | non-bridging | | | endo-cyclic | | exo-cyclic | |
	P-O(C)	$P-O(H)/P_{..}^-O$	HB	P-O:Mg	P-O	HB	P-O	HB
$P-O(H)/P^-O$	1.716	1.547	-	-	1.946	-	1.803	-
$[Mg(H_2O)_5(EPA)]$	1.665	1.572	+	1.574	1.744	-	1.874	+
$[Mg(H_2O)_4(b\text{-}EPA)]$	1.651	-	-	1.567	1.901	+	1.768	+
$[Mg(H_2O)_3(OH)(b\text{-}EPA)]^{1-}$	1.673	-	-	1.550	1.981	+	1.778	+
$[EPAH_2]$	1.653	1.630	-	-	1.727	-	1.674	-
$[EPAH]^-(\uparrow)$	1.706	1.661	-	-	1.893	-	1.715	-
$[EPAH]^-(\downarrow)$	1.714	1.665	-	-	1.779	-	1.790	-
$[Mg(H_2O)_5(EPAH)]^{1+}_{exo}$	1.641	1.693	+	1.547	1.743	-	1.740	+
$[Mg(H_2O)_5(EPAH)]^{1+}_{endo}$	1.626	1.679	+	1.540	1.938	+	1.649	-
$[Mg(H_2O)_4(OH)(EPAH)]$	1.663	1.642	-	1.542	1.827	+	1.705	-

Bridging/non-bridging distinguishes between oxygens which are bridged between a P and C atom versus an O which is bonded only to P (or in the case of neutral phosphates bound to H as well). $[EPA]^{2-}_{aq}$ optimization was preformed using the PCM solvation model (see text). ($\uparrow$) or ($\downarrow$) indicate the orientation of the proton on

the non-bridging O relative to the ethylene ring. Columns headed by HB indicate the presence (+) or absence (-) of a hydrogen bond between a Mg^{2+}-water and the phosphorane oxygen. Deviations are shown in parentheses. Subscripts exo/endo distinguish which axial oxygen atom is hydrogen bonded

EPA^{2-}, which suggests that a similar contraction occurs for di-anionic phosphoranes in solution as well.

Coordination distances for di-anionic and mono-anionic phosphoranes are shown in Table 2. A recent high-resolution (1.2 Å) crystal structure of β-phospho-glucomutase [72] showed Mg^{2+} bound to a di-anionic phosphorane at a distance of 2.16 Å, which is close to the distance of 2.03 Å observed for [Mg(HOH)$_5$(EPA)] in this study.

Thermodynamic quantities

Table 3 lists thermodynamic quantities for ligand substitution reactions that involve replacement of a biological ligand coordinated to a hydrated Mg^{2+} with a water molecule. Understanding which factors make binding to phosphates and phosphoranes more favorable offers many insights into how and why metal binding to nucleic acids occurs.

Ligand substitution reactions

In this section, ligand substitution reactions are examined of the form:

$$[Mg(H_2O)_6]^{2+} + L^{q-} \rightarrow [Mg(H_2O)_5(L)]^{2-q} + H_2O$$

(8)
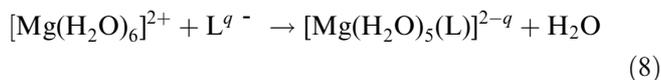
In the gas phase, binding of a negatively charged ligand to penta-hydrated Mg^{2+} is highly favorable. The smaller and more negatively charged the ligand, the more favorable the water ligand substitution. For example, Mg^{2+} binding to -2 charged EPA^{2-} is most favorable and hydroxide, which has a higher charge density due to its small size and hardness, is more strongly stabilized by Mg^{2+} binding than larger or more neutral ligands. Reactions involving neutral ligand binding to Mg^{2+} have considerably more positive free energy than negatively charged ligands, however, the binding interaction is still favorable in the gas phase. In comparison with other biological ligands having a -1 charge, phosphates have less affinity for binding to Mg^{2+} than smaller ligands such as OH$^-$ and CH$_3$O$^-$. Phosphorane ligands of similar charge, although larger in size, have a more negative free energy than phosphates, in part due to the variety of hydrogen bonding interactions formed upon Mg^{2+} binding as was discussed above. Cyclic phosphate compounds have a less positive entropic contribution than acyclic ones, whether bound or unbound to hydrated Mg^{2+}.

Substitutions in which a monodentate ligand displaces a H$_2$O ligand to bind Mg^{2+} bidentate are unfavorable in the gas phase. While the entropic contribution of the water displacement is highly favorable due to a chelate effect, the internal energy is very unfavorable due to increased structural strain. For phosphate ligands, this internal energy is sufficiently positive to prevent a favorable free energy of reaction (Table 3). For phosphorane binding, the smaller equatorial O–P–O angle of [Mg(H$_2$O)$_5$(b-EPA)] permits a slightly more favorable internal energy of binding and weakly negative free energy in the gas phase.

Table 3 Ligand substitution energies (kcal/mol)

L	Gas phase properties				ΔG_{aq}	
	ΔE	ΔH	$-T\Delta S$	ΔG	PCM	COSMO
mono-dentate reactions						
CH$_3$COOH	−12.93	−13.49	1.33	−12.16	6.18	5.59
H$_3$PO$_4$	−22.56	−23.28	1.41	−21.86	1.93	1.67
DMPH	−28.77	−29.33	1.34	−27.99	5.47	4.60
EPH	−29.19	−29.63	1.37	−28.26	1.08	1.43
OH$^-$	−229.69	−230.03	−0.36	−230.39	−4.45	6.23
CH$_3$O$^-$	−218.66	−217.17	0.52	−216.65	−7.47	−0.18
CH$_3$COO$^-$	−203.76	−204.78	2.22	−202.56	−5.81	−0.88
EPAH$^-$	−205.14	−204.47	4.09	−200.38	−6.96	−2.84
EP$^-$	−197.98	−198.15	3.86	−194.29	−5.61	−2.37
H$_2$PO$_4^-$	−196.06	−196.58	2.52	−194.06	−6.21	−3.48
HPO$_4^{2-}$	−396.14	−398.62	6.08	−392.53	−6.97	1.04
EPA^{2-}	−395.72	394.63	5.78	−388.86	−6.12	4.79
bi-dentate reactions						
b-DMP$^-$	18.42	16.98	−11.23	5.75	−0.13	−0.94
b-EP$^-$	14.51	13.22	−11.46	1.77	−5.54	−5.95
b-EPA^{2-}	8.31	7.25	−11.07	−3.82	−8.71	−9.13

Mono-dentate reactions are of the form [Mg(H$_2$O)$_6$]$^{2+}$ + L^{-q} $\rightarrow$ [Mg(H$_2$O)$_5$(L)]$^{2-q}$ + H$_2$O and bi-dentate reactions are of the form [Mg(H$_2$O)$_5$(L)]$^{-q}$ $\rightarrow$ [Mg(H$_2$O)$_4$(b-L)]$^{-q}$ + H$_2$O where b-L indicates a ligand bound bi-dentate to Mg^{2+}. Due to the instability of [EPA]$^{2-}$ in the gas phase, the structure was first optimized using the PCM solvation model (see text). Single point energies were then calculated for the optimized structure in the gas phase. Columns headed with PCM and COSMO indicate ΔG_{aq} single point calculations performed with the PCM and COSMO solvation models

The ΔG_{sol} (see Eq. 1) for the ligand substitution reactions in Table 3 were highly positive for all but the monodentate to bidentate substitutions, destabilizing the ΔG_{aq} values relative to the ΔG_{gas} values. There is a large variation in the ΔG_{sol} for some complexes solvated with the PCM versus the COSMO methods. This is due to the error in solvation energy calculated by the implicit solvation model for some ligands. Small, negatively charged ligands showed the largest deviations from experimental values. Hydroxide, for instance, has a ΔG_{sol} of -100.17 kcal/mol for PCM and -109.90 kcal/mol for COSMO, and methoxide has a ΔG_{sol} of -80.59 kcal/mol for PCM and -87.22 kcal/mol for COSMO. The experimental values [73] for ΔG_{sol} of these two ligands are -110 kcal/mol and -95 kcal/mol, respectively.

Lg^{2+} binding to deprotonated phosphates and other mono-anionic ligands are stable in aqueous solution, while deprotonated phosphorane is unstable according to the COSMO model. This may be due once again to the high stability of such a negatively charged ligand when unbound in solution. Bidentate bound ligands change from being unstable in the gas phase to stable in solution. Solvation partially alleviates repulsion between negatively charged ligands in close proximity. Phosphorane ligand binding, which is unfavorable when bound monodentate, is more favorable compared with other solvated complexes when bound bidentate.

Bridging di-metal Mg(II) ion complexes

Under considerable debate for many metal-dependent ribozymes is the question of how many and in what way metal ions play a chemical versus a structural role. Mechanisms for the group I intron, RNase P, and hammerhead ribozymes have all been proposed to have more than one metal ion directly participating in catalysis [22, 74, 75, 76, 77, 78]. X-ray crystallography of a freeze-trapped hammerhead ribozyme intermediate [79] identified six possible Mg^{2+} ion binding positions. Two of these positions were located very near the active site and were suggested to be involved with the required 2'-OH deprotonation of nucleotide C_{17} [64, 79]. However, none of the hammerhead structures in the original crystallographic study [79], including that of the freeze-trapped intermediate, had the 2'-hydroxide poised for in-line nucleophilic attack to the scissile phosphate. Further pioneering work was able to capture the ribozyme–product complex [80] and a chemically trapped "late intermediate" [81] that does have the 2'-hydroxide positioned for nucleophilic attack. These structures, along with a wealth of other biophysical and biochemical data [19], have lead to the suggestion that there is a critical pH-dependent conformational change that must occur [82], and that this conformational step might be the rate-controlling step of ribozyme cleavage. Although it has been further suggested that deprotonation at the 2'-position might trigger the conformational change [81],

all the pH-dependent factors that might influence the conformational step have not been conclusively identified. Moreover, questions remain as to the specific role played by the metal ions in both the conformational and chemical steps of the reaction, since their positions are in some cases significantly different in the different crystallographic structures that represent different steps along the catalytic path. For the chemical step, models have been proposed for both a single-metal and double-metal ion mechanisms [83, 84]. One model that has been recently proposed for the chemically active ribozyme involves a single metal ion that bridges the A9 residue and a non-bridging oxygen of the scissile phosphate [85, 86]. Another suggests a di-metal complex bridged by a hydroxide, based on the 4.25 Å distance between Mg^{2+} sites 1 and 6 in the Scott et al. [79] 301D crystal structure. These largely experimental studies have been complemented by molecular dynamics simulations that model the di-metal bridge structure. One such study, based on empirical molecular simulation force fields, suggested that without a μ-bridging OH^- placed between these two ions, electrostatic repulsion would lead to their dissociation [87, 88]. Upon a flip of the ribose pucker from C3'-endo to C2'-endo the di-Mg^{2+} complex was in a position such that the OH^- could act as a base to aid in the 2'-OH deprotonation [88].

The present work directly characterizes the structure and stability of di-Mg^{2+} complexes based on high-level density-functional calculations, and confirms the requirement that a di-Mg^{2+} bridge complex is stable in the presence of a μ-bridging hydroxide, but unstable in the presence of a μ-bridging water molecule. This result may be significant since the pK_a of such a di-Mg^{2+} complex is expected to be considerably lower than that of a single Mg^{2+} ion, and protonation at the μ-bridging hydroxide position (in the absence of other stabilizing factors) would lead to dissociation of the complex. It is noteworthy that the Mg^{2+} ion bound to the pro-R oxygen (site 6) in the crystallographic structure of the freeze-trapped intermediate [79], which is suspected to form a di-metal bridge with a Mg^{2+} located 4.25 Å away (site 1), occurs only at elevated pH (8.5) and is not present in the lower pH "ground state" structure. It is possible, therefore, that at lower pH a μ-bridging hydroxide between these metal ions becomes protonated, leading to destabilization of the di-metal complex and Mg^{2+} binding at the site 6 position. Although the di-metal bridge complexes are predicted to bind more strongly with mono-anionic phosphates and phosphoranes than single Mg^{2+} ions, the calculated binding affinity of a single Mg^{2+} ion is sufficiently strong that a single-metal mechanism that occurs via direct inner-sphere coordination to the non-bridging pro-R oxygen, as supported by recent spectroscopic evidence [17], cannot be discounted.

To better understand how a di-Mg^{2+} complex might facilitate phosphate hydrolysis reactions, the structure, stability, and binding energy of di-Mg^{2+} complexes are examined and compared to those of a single metal ion.

Structure

Ligand coordination distances (Table 4) to the di-Mg^{2+} complexes studied are larger than for the single Mg^{2+} complexes, ranging from 0.04 Å to 0.08 Å longer. The average water coordination distance to Mg^{2+} increased also from 0.02 Å to 0.04 Å. Hydroxide, the tightest binding ligand for both the single and di-Mg^{2+} complexes, bound 0.067 Å less tightly for the di-Mg^{2+} complex. Di-Mg^{2+} complexes with anionic ligand binding have slighter contractions, relative to single Mg^{2+} ion complexes, than neutral ligands. This derives from a combination of higher charge and hydrogen bonding interactions present in these systems (Fig. 4). Each hydrogen bond a Mg^{2+}-bound water makes with a phosphate oxygen results in a small amount of electron density transfer to the water, which then causes a decrease in coordination distance with Mg^{2+}. All of the phosphate-bound di-Mg^{2+} complexes studied have between 2–4 hydrogen bond interactions present, resulting in a smaller average water coordination distance overall for the di-Mg^{2+} complexes (Table 4).

Changes in phosphate geometry (Table S7) induced by Mg^{2+} binding were in most cases similar between single- and di-Mg^{2+} complexes. The largest difference was seen in the magnitude of the Mg^{2+} coordinating P–O bond for $[Mg(HOH)_5\text{-}(\mu\text{-OH})\text{-}Mg(HOH)_4(EP)]^{2+}$, in which hydrogen bonding interactions play a significant role in ligand stabilization. For this complex, the coordinating oxygen is hydrogen bonded with a Mg^{2+}-bound water as well (Fig. 4), resulting in a P–O bond that is 0.03 Å larger than for $[Mg(HOH)_5\text{-}(\mu\text{-OH})\text{-}Mg(HOH)_4(DMP)]^{2+}$. A unique hydrogen bonding interaction is seen for $[Mg(HOH)_5\text{-}(\mu\text{-OH})\text{-}Mg(HOH)_4(DMP)]^{2+}$ as well, in which the ligand is stabilized by two separate Mg^{2+} waters. The resulting constrained geometry caused by this double interaction may be responsible for the significant deviation of 0.04 Å seen between the ligand coordination distance of $[Mg(HOH)_5\text{-}(\mu\text{-OH})\text{-}Mg(HOH)_4(DMP)]^{2+}$ as compared with $[Mg(HOH)_5\text{-}(\mu\text{-OH})\text{-}Mg(HOH)_4(EP)]^{2+}$.

Energies

Ligand substitution reactions with water for the di-Mg^{2+} complexes studied are more favorable than for single Mg^{2+} complexes in both the gas and aqueous phases. Relative free energy differences between competing ligand substitutions are more favorable as well. For example, while the gas-phase free energy difference between EP^- ligand substitution and OH^- substitution is only −36.1 kcal/mol when bound to a single Mg^{2+} ion, the energy difference increases to −43.5 kcal/mol for di-Mg^{2+} binding (Tables 3 and 5). Likewise, the energy difference between DMPH and DMP^- binding increases from −168.9 kcal/mol for single Mg^{2+} complexes to −223.2 kcal/mol for di-Mg^{2+} complexes.

Table 4 Geometries of hydrated di-Mg^{2+} complexes with biological ligand binding (Å)

L^{-q}	$P-O(H)/P_{..}^-O$	$Mg2+\cdots\mu$-OH	$Mg\cdot L$	$Mg^{2+}\cdots Mg^{2+}$	$Mg^{2+}\cdots OH\cdots Mg^{2+}$
H_2O	2.155(0.032)	2.033(0.000)	2.155	3.97	155.58
$DMPH_{g\text{-}g}$	2.152(0.036)	2.012(0.000)	2.112	3.79	139.65
EPH	2.152(0.036)	2.017(0.008)	2.113	3.79	139.89
OH^-	2.154(0.023)	2.015(0.011)	2.023	3.57	124.85
$DMP^-_{g\text{-}g}$	2.148(0.019)	2.022(0.009)	2.047	3.81	140.74
EP^-	2.146(0.051)	2.016(0.017)	2.089	3.68	131.92
EPA^{2-}	2.142(0.041)	2.048(0.014)	2.124	3.57	121.26

Structures are of the form $[Mg(H_2O)_5\text{-}(\mu\text{-OH})\text{-}Mg(H_2O)_4(L)]^{3-q}$. For DMP compounds, the subscripts g-g indicates the gauche-gauche conformation. Deviations are shown in parentheses

Fig. 4 $[Mg(HOH)_5\text{-}(\mu\text{-OH})\text{-}Mg(HOH)_4(EP)]^{2+}$ and $[Mg(HOH)_5\text{-}(\mu\text{-OH})\text{-}Mg(HOH)_4(EPA)]^+$ structures
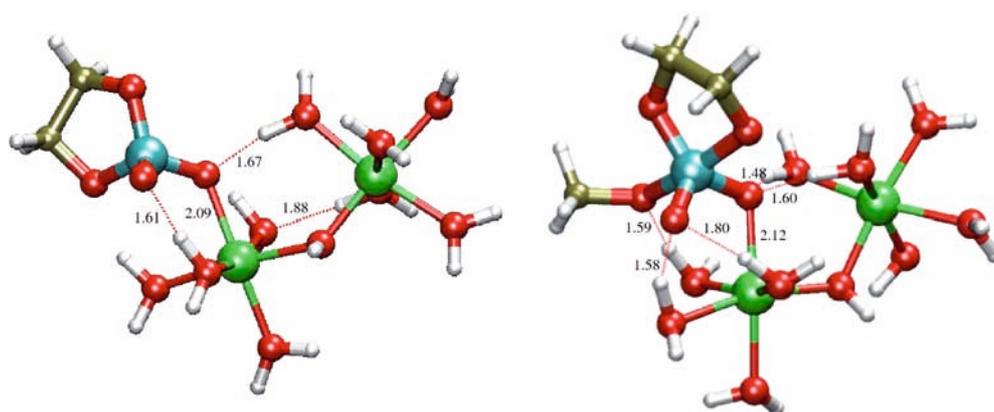
Table 5 Di-metal ligand substitution energies (kcal/mol)

| L | Gas phase properties | | | | ΔG_{aq} | |
	ΔE	ΔH	$-T \cdot S$	ΔG	PCM	COSMO
DMPH	−33.98	−34.12	4.51	−29.60	5.15	4.83
EPH	−32.94	−32.97	4.17	−28.80	2.76	3.29
OH⁻	−293.07	−293.19	4.19	−288.99	−23.58	−6.70
DMP⁻	−258.53	−258.09	5.24	−252.85	−10.36	−6.36
EP⁻	−253.51	−253.04	7.58	−245.46	−9.04	−3.91

Reactions are of the form $[Mg(H_2O)_5\text{-}(\mu\text{-}OH)\text{-}Mg(H_2O)_5]^{3+} + L^{-q} \rightarrow [Mg(H_2O)_5\text{-}(\mu\text{-}OH)\text{-}Mg(H_2O)_4(L)]^{3-q} + H_2O$. Columns headed with PCM and COSMO indicate ΔG_{aq} single point calculations performed with the PCM and COSMO solvation models

As found with single Mg^{2+} ion complexes, ligand binding in aqueous solution is much less favorable than in the gas phase. In many cases, ligand binding to di-Mg^{2+} has a less favorable ΔG_{aq} than single Mg^{2+} binding reactions. This is due in part to the increased solvent stabilization of the uncomplexed di-Mg^{2+} system. When a smaller ligand such as OH^- is substituted, a more favorable ΔG_{aq} value of −6.70 kcal/mol for di-Mg^{2+} ligand substitution is observed.

Conclusions

In this work, we have extended the study of divalent metal ion binding with ligands relevant to phosphate hydrolysis through theoretical investigation of Mg^{2+} ion binding to phosphates, phosphoranes, and other biological ligands. Mg^{2+} binding was found to induce significant geometry changes of both phosphate and especially phosphorane structure. In the case of phosphates, large contractions of the bridging P–O bonds were observed upon Mg^{2+} binding. Comparison of crystal structures for the hammerhead ribozyme with and without Mg^{2+} bound at the scissile phosphate [79] do not show this trend. In the 301D crystal structure, however, Mg^{2+} is coordinated to the *pro-R* oxygen at a distance of 2.427 Å, which is much larger than the distance of 2.005 Å observed in the present study for $[Mg(HOH)_5(DMP)]^+$. Furthermore, the higher resolution crystal structure of β-phosphoglucomutase [72] shows Mg^{2+} bound to a di-anionic phosphorane at a distance of 2.16 Å, which is close to the distance of 2.03 Å observed for $[Mg(HOH)_5(EPA)]$ in this study.

Hydrogen bonding interactions between the phosphate ligands and Mg^{2+} waters were present in many cases, but were weak in most cases and appear to play a relatively minor role in the overall complex stabilization. In the case of phosphoranes, however, hydrogen bonding interactions are important for stabilization of the high charge of the non-bridging and axial oxygen atoms. The presence or absence of a hydrogen bonding interaction at an exocyclic or endocyclic axial oxygen plays a key role in the type of intermediate that is stabilized. Hydrogen bonding at these positions lengthens the corresponding P–O bond, thus stabilizing an intermediate of either ring cleavage or closure.

The di-anionic form of methyl(ethylene)phosphorane (EPA^{2-}) is unstable in the gas phase. When bound to Mg^{2+}, however, a highly stable complex is formed. Some important differences exist for ligand binding between the gas and solution phases. In the gas phase, with the exception of bidentate binding phosphates, all ligands have favorable substitution with a Mg^{2+} bound water. In solution phase, neutral ligand substitutions become unfavorable and bidentate binding becomes favorable. Most mono-anionic ligand substitutions remain favorable, although to a considerably lower degree than that seen in the gas phase. However, di-anionic substitution reactions with ligands such as phosphorane were predicted by COSMO to be unfavorable in solution phase. Despite a very favorable free energy in the gas phase, the solvation energy of the Mg^{2+} bound complex is less favorable than for the ligand alone. This suggests that phosphates may bind Mg^{2+} more strongly than phosphoranes. In hammerhead ribozyme it is seen that the active site bound Mg^{2+} is no longer present on the product structure. This lower affinity for Mg^{2+} to phosphorane could explain why the metal ion is released as the transition state geometry of the reaction is reached.

Bridging di-Mg^{2+} complexes have similar trends to those seen for single Mg^{2+} complexes. Some variation in degree of the effects due to binding was seen, however. Ligand substitutions of Mg^{2+} waters with phosphates were more favorable for di-Mg^{2+} complexes. Ligand coordination distances as well tended to be larger than those seen for the single Mg^{2+} complexes.

The results presented here provide quantitative insight into the structure and stability of Mg^{2+} binding to phosphate and phosphorane compounds relevant for the study of RNA catalysis. Additionally, this work serves to further the goal of developing new semi-empirical Hamiltonians which can be applied to large-scale linear-scaling electronic structure calculations of ribozyme systems.

References

1. Cowan JA (1998) Chem Rev 98:1067–1087
2. Takagi Y, Ikeda Y, Taira K (2004) Top Curr Chem 232:213–251
3. Strajbl M, Shurki A, Warshel A (2003) Proc Natl Acad Sci USA 100:14834–14839
4. Florián J, Goodman MF, Warshel A (2003) J Am Chem Soc 125:8163–8177
5. Tiraboschi G, Gresh N, Giessner-Prettre C, Pedersen LG, Deerfield DW (2000) J Comput Chem 21:1011–1039
6. Mercero JM, Fowler JE, Ugalde JM (1998) J Phys Chem A 102:7006–7012
7. Florián J, Warshel A (1998) J Phys Chem B 102:719–734
8. Tole P, Lim C (1994) J Am Chem Soc 116:3922–3931
9. Dejaegere A, Liang XL, Karplus M (1994) J Chem Soc Faraday Trans 90:1763–1767
10. Range K, McGrath MJ, Lopez X, York DM (2004) J Am Chem Soc 126:1654–1665
11. Lopez X, Dejaegere A, Karplus M (2001) J Am Chem Soc 123:11755–11763
12. Mercero JM, Barrett P, Lam CW, Fowler JE, Ugalde JM, Pedersen LG (2000) J Comput Chem 21:43–51
13. Fothergill M, Goodman MF, Petruska J, Warshel A (1995) J Am Chem Soc 117:11619–11628
14. Cowan JA (1997) J Biol Inorg Chem 2:168–176
15. Torres RA, Himo F, Bruice TC, Noodleman L, Lovell T (2003) J Am Chem Soc 125:9861–9867
16. Schneider B, Kabeláč M, Hobza P (1996) J Am Chem Soc 118:12207–12217
17. Cunningham LA, Li J, Lu Y (1998) J Am Chem Soc 120:4518–4519
18. Maderia M, Hunsicker LM, DeRose VJ (2000) Biochemistry 39:12113–12120
19. Scott WG (1999) Q Rev Biophys 32:241–294
20. Wilson TJ, Lilley DMJ (2002) RNA 8:587–600
21. Hampel A, Cowan JA (1997) Chem Biol 4:513–517
22. Smith D, Pace NR (1993) Biochemistry 32:5273–5281
23. Eckstein F, Bramlage B (1999) Biopolymers 52:147–154
24. Åqvist J, Warshel A (1990) J Am Chem Soc 112:2860–2868
25. Shan S, Kravchuk AV, Piccirilli JA, Herschlag D (2001) Biochemistry 40:5161–5171
26. Takagi Y, Taira K (2002) J Am Chem Soc 124:3850–3852
27. Bruice TC, Tsubouchi A, Dempcy RO, Olson LP (1996) J Am Chem Soc 118:9867–9875
28. Peracchi A, Beigelman L, Scott EC, Uhlenbeck OC, Herschlag D (1997) J Biol Chem 272:26822–26826
29. Taraszka JA, Li J, Clemmer DE (2000) J Phys Chem B 104:4545–4551
30. Warshel A (2003) Annu Rev Biophys Biomol Struct 32:425–443
31. Warshel A, Levitt M (1976) J Mol Biol 103:227–249
32. Åqvist J, Warshel A (1993) Chem Rev 93:2523–2544
33. Gao J, Truhlar DG (2002) Annu Rev Phys Chem 53:467–505
34. Hutter MC, Reimers JR, Hush NS (1998) J Phys Chem B 102:8080–8090
35. Hutter MC, Hughes JM, Reimers JR, Hush NS (1999) J Phys Chem B 103:4906–4915
36. Frisch MJ, Trucks GW, Schlegel HB, Scuseria GE, Robb MA, Cheeseman JR, Montgomery JA Jr, Vreven T, Kudin KN, Burant JC, Millam JM, Iyengar SS, Tomasi J, Barone V, Mennucci B, Cossi M, Scalmani G, Rega N, Petersson GA, Nakatsuji H, Hada M, Ehara M, Toyota K, Fukuda R, Hasegawa J, Ishida M, Nakajima T, Honda Y, Kitao O, Nakai H, Klene M, Li X, Knox JE, Hratchian HP, Cross JB, Adamo C, Jaramillo J, Gomperts R, Stratmann RE, Yazyev O, Austin AJ, Cammi R, Pomelli C, Ochterski JW, Ayala PY, Morokuma K, Voth GA, Salvador P, Dannenberg JJ, Zakrzewski VG, Dapprich S, Daniels AD, Strain MC, Farkas O, Malick DK, Rabuck AD, Raghavachari K, Foresman JB, Ortiz JV, Cui Q, Baboul AG, Clifford S, Cioslowski J, Stefanov BB, Liu G, Liashenko A, Piskorz P, Komaromi I, Martin RL, Fox DJ, Keith T, Al-Laham MA, Peng CY, Nanayakkara A, Challacombe M, Gill PMW, Johnson B, Chen W, Wong MW, Gonzalez C, Pople JA (2003), Gaussian 03 R B01. Gaussian, Pittsburgh
37. Becke AD (1993) J Chem Phys 98:5648–5652
38. Lee C, Yang W, Parr RG (1988) Phys Rev B 37:785–789
39. Helgaker T, Watson M, Handy NC (2000) J Chem Phys 113:9402–9409
40. Bauernschmitt R, Ahlrichs R (1996) J Chem Phys 104:9047–9052
41. Seeger R, Pople JA (1977) J Chem Phys 66:3045–3050
42. Curtiss LA, Raghavachari K, Trucks GW (1991) J Chem Phys 94:7221–7230
43. Tomasi J, Persico M (1994) Chem Rev 94:2027–2094
44. Cossi M, Barone V, Cammi R, Tomasi J (1996) Chem Phys Lett 255:327–335
45. Mineva T, Russo N, Sicilia E (1998) J Comput Chem 19:290–299
46. Cossi M, Scalmani G, Rega N, Barone V (2002) J Chem Phys 117:43–54
47. Barone V, Cossi M (1998) J Phys Chem A 102:1995–2001
48. Klamt A (1995) J Phys Chem 99:2224–2229
49. Andzelm J, Kölmel C, Klamt A (1995) J Chem Phys 103:9312–9320
50. Pierotti RA (1976) Chem Rev 76:717–726
51. Barone V, Cossi M, Tomasi J (1997) J Chem Phys 107:3210–3221
52. Floris FM, Tomasi J, Pascual-Ahuir JL (1991) J Comput Chem 12:784–791
53. Miertuš S, Scrocco E, Tomasi J (1981) Chem Phys 55:117–129
54. Cammi R, Tomasi J (1995) J Comput Chem 16:1449–1458
55. Klamt A, Schüürmann G (1993) J Chem Soc Perkin Trans 2 2:799–805
56. York DM, Karplus M (1999) J Phys Chem A 103:11060–11079
57. Cramer CJ (2002) Essentials of computational chemistry: theories, models. Wiley, Chichester
58. Bock CW, Kaufman A, Glusker JP (1994) Inorg Chem 33:419–427
59. Katz AK, Glusker JP, Beebe SA, Bock CW (1996) J Am Chem Soc 118:5752–5763
60. Pye CC, Rudolph WW (1998) J Phys Chem A 102:9933–9943
61. Pavlov M, Siegbahn PEM, Sandström M (1998) J Phys Chem A 102:219–228
62. Saito H, Suga H (2002) Nucleic Acids Res 30:5151–5159
63. Vaidya A, Suga H (2001) Biochemistry 40:7200–7210
64. Markley JC, Godde F, Sigurdsson ST (2001) Biochemistry 40:13849–13856
65. Dahm SC, Uhlenbeck OC (1991) Biochemistry 30:9464–9469
66. Marcus Y (1988) Chem Rev 88:1475–1498
67. Dudev T, Lim C (1999) J Phys Chem A 103:8093–8100
68. Reed AE, Weinstock RB, Weinhold F (1985) J Chem Phys 83:735–746
69. Zhou D, Taira K (1998) Chem Rev 98:991–1026
70. Lopez X, Schaefer M, Dejaegere A, Karplus M (2002) J Am Chem Soc 124:5010–5018
71. Holmes RR (1978) J Am Chem Soc 100:433–446
72. Lahiri SD, Zhang G, Dunaway-Mariano D, Allen, KN (2003) Science 299:2067–2071
73. Li J, Zhu T, Hawkins GD, Winget P, Liotard DA, Cramer CJ, Truhlar DG (1999) Theor Chem Acc 103:9–63
74. Hertweck M, Mueller MW (2001) Eur J Biochem 268:4610–4620
75. Pontius BW, Lott WB, von Hippel PH (1997) Proc Natl Acad Sci USA 94:2290–2294
76. Torres RA, Bruice TC (1998) Proc Natl Acad Sci USA 95:11077–11082
77. Sjögren AS, Pettersson E, Sjöberg BM, Strömberg R (1997) Nucleic Acids Res 25:648–653
78. Warnecke JM, Fürste J, Peter H, Wolf-Dietrich E, Volker A, Hartmann RK (1996) Proc Natl Acad Sci USA 93:8924–8928
79. Scott WG, Murray JB, Arnold JRP, Stoddard BL, Klug A (1996) Science 274:2065–2069

80. Murray JB, Szöke H, Szöke A, Scott WG (2000) Mol Cell 5:279–287
81. Murray JB, Terwey DP, Maloney L, Karpeisky A, Usman N, Beigelman L, Scott WG (1998) Cell 92:665–673
82. Murray JB, Dunham CM, Scott WG (2002) J Mol Biol 315:121–130
83. Zhou D, Zhang L, Taira K (1997) Proc Natl Acad Sci USA 94:14343–14348
84. Kuimelis RG, McLaughlin LW (1996) Biochemistry 35:5308–5317
85. Murray JB, Scott WG (2000) J Mol Biol 296:33–41
86. Murray JB, Scott WG (2000) J Mol Biol 304:681
87. Hermann T, Auffinger P, Scott WG, Westhof E (1997) Nucleic Acids Res 25:3421–3427
88. Hermann T, Auffinger P, Westhof E (1998) Eur Biophys J 27:153–165